A Unified Approach for Spatial and Angular Super-Resolution of Diffusion Tensor MRI

Shi Yin[1], Xinge You[1(✉)], Weiyong Xue[1], Bo Li[1], Yue Zhao[1], Xiao-Yuan Jing[2], Patrick S.P. Wang[3], and Yuanyan Tang[4]

[1] School of Electronic Information and Communications,
Huazhong University of Science and Technology, Wuhan, China
youxg@hust.edu.cn
[2] School of Computer, Wuhan University, Wuhan, China
[3] College of Computer and Information Science,
Northeastern University, Boston, USA
[4] Faculty of Science and Technology, University of Macau, Macau, China

Abstract. Diffusion magnetic resonance imaging (dMRI) can provide quantitative information with which to visualize and study connectivity and continuity of neural pathways in nervous systems. However, the very subtle regions and multiple intra-voxel orientations of water diffusion in brain cannnot accurately be represented in low spatial resolution imaging with tensor model. Yet, the ability to trace and describe such regions is critical for some applications such as neurosurgery and pathologic diagnosis. In this paper, we proposed a new single image acquisition super-resolution method to increase both the spatial and angular resolution of dMRI. The proposed approach called single dMRI super-resolution reconstruction with compressed sensing (SSR-CS), uses a low number of single diffusion MRI in different gradients. This acquisition scheme is effectively in reducing acquisition time while improving the signal-to-noise ratio (SNR). The proposed method combines the two strategies of nonlocal similarity reconstruction and compressed sensing reconstruction in a sparse basis of spherical ridgelets to reconstruct high resolution image in k-space with complex orientations. The split Bregman approach is introduced for solving the SSR-CS problem. The performance of the proposed method is quantitatively evaluated on simulated diffusion MRI, using both spatial and angular reconstruction evaluating indexes. We also compared our method with some other dMRI super resolution methods.

Keywords: Diffusion magnetic resonance imaging (dMRI) · Tensor model · Single dMRI super-resolution · Compressed sensing (CS) · Sparse representation

1 Introduction

Diffusion tensor imaging enables the reconstruction of information revealing the shape, the coherence and the integrity of brain tissue microstructure which can

be indirectly analyzed through the assessment of motion of water molecules [1]. This technique has been applied widely in vivo analysis of white matter architecture and has recently been applied to the study of gray matter. Moreover, diffusion tensor imaging has been used to study a large range of neurological disease, or to quantify other causes of tissue degradations such as epilepsy and malformations of cortical development [2]. It has been shown that at a voxel resolution of around 2–3 mm, a simple tensor model used to track the major white matter pathways in the human brain [3]. Despite its interesting properties, diffusion tensor imaging is an inherently low signal-to-noise ratio (SNR) technique and yields to relatively poor spatial resolution [4]. Besides, the tensor model fails to accurately track through regions with more complex fiber arrangements such as crossing, fanning and branching.

It has been shown that the limited spatial and angular resolution introduces a bias in diffusion parameter estimation [4]. Therefore, to improve the sensitivity and robustness of studies based on diffusion tensor imaging, high spatial and angular resolution (HSAR) diffusion MRI with high SNR has to be considered. Such HSAR diffusion MRI with high SNR could provide a better sensitivity for the brain microstructure. However the acquisition of such HSAR diffusion MRI remains a challenging problem in clinical conditions since the improvement in HSAR is obtained at the cost of either lower SNR, longer acquisition time or both [5]. For example, to resolve the crossing fiber direction one can apply more sophisticated local models like the DSI or HARDI, a low spatial resolution of about 3 mm is used to achieve sufficient SNR to enable the acquisition of a high number of diffusion directions and multiple b-values, thereby resolving crossing fiber directions [6]. However, this improvement of high angular resolution with high SNR is obtained at the cost of the longer acquisition time and the spatial resolution.

To enable acquisition of high spatial diffusion MRI without long acquisition times, super-resolution (SR) acquisition techniques have been investigated in the past. Some possible strategies consist in fusing several anisotropic acquisitions with a high in-plane resolution only along one axis [7–10]. In contrast to SR acquisition techniques that require specific acquisitions protocols of multiple LR images, there exists also a category of single image SR methods [4]. Since single image SR techniques are pure post-processing methods and thus are totally independent from the acquisition protocol. The main idea is to use the image content to reconstruct information at higher-resolution. Besides, another SR method for diffusion MRI has been proposed. The main idea is to use an HR image to drive the reconstruction of another modality (e.g. using $\mathbf{B_0}$ image) [4]. However, this type of method is built on assumption that the two modalities have the similar image structures. Another problem in these methods is that few of them have considered the angular resolution. Only increasing the spatial resolution cannot break through the limitations of the tensor model. Besides, the ignorance of angular resolution also means the ignorance of the relationship between the diffusion images of different directions.

In this paper, we investigate the possibility to increase both the spatial and the angular resolution of diffusion imaging using single image SR method and compressed sensing. We proposed a unified approach to reconstruct HSAR image using the single dMRI set which are undersampled in k-space and q-space. Then we acquire the corresponding probabilistic orientation function (ODF) through the HSAR dMRI. To quantitatively assess the performance of the proposed method, we use the simulated dMRI. Some other super spatial dMRI methods are also evaluated for these data for comparing the high spatial reconstruction performance. We should note that, to the best of our knowledge, this is a first instance of using the single diffusion dMRI set to reconstruct HSAR dMRI.

The contributions of this work are twofold.

(1) The proposition of a new SSR-CS method to reconstruct the HSAR dMRI.
(2) The introduction of an efficient optimization algorithm for solving the SSR-CS model.

The remainder of the paper is organized as follows. Section 2 briefly reviews the background of the approach. Section 3 presents the proposed SSR-CS model. The experimental results are demonstrated in Sect. 4 in comparing with the state-of-the-art SR methods. Section 5 concludes the paper.

2 Background

In this section, we provide a brief background on diffusion tensor imaging and spherical ridgelets which will be used subsequently in our proposed SSR-CS algorithm.

2.1 3D Diffusion MRI

In diffusion MRI, measurements are commonly made using the pulsed gradient spin echo (PGSE) method, which samples the Fourier transform of the ensemble average diffusion propagator (EAP) $P(\mathbf{r})$, two magnetic field gradient pulses of duration δ and separation Δ are introduced to the simple spin-echo sequence [11, 12]. Assuming rectangular pulse profiles, the associated diffusion direction is $\mathbf{q} = \gamma\delta\mathbf{g}$, where $\mathbf{g}$ is the component of the gradient in the direction of the fixed field $\mathbf{B}_0$ and γ is the gyromagnetic ratio. The diffusion MRI measurement $S(\mathbf{q}; \mathbf{r})$is defined at each location $\mathbf{r}$ of a finite regular image grid in three-dimensional space and depends on the gradient direction $\mathbf{q}$. For each vector $\mathbf{q}_k$, the diffusion MRI measurement $S(\mathbf{q}_k)$ is a 3D DWI. The normalized $S^*(\mathbf{q}_k)$ is given by

$$S^*(\mathbf{q}_k) = (S(\mathbf{0}))^{-1}S(\mathbf{q}_k) \tag{1}$$

$S(\mathbf{0})$denotes the diffusion signal obtained in the absence of diffusion encoding (i.e.,the so-called "$\mathbf{B}_0$-image"). when the $\Delta^{-1}\delta$ is negligible,

$$S^*(\mathbf{q}_k) = \int_{\mathbf{r}\in\mathbb{R}^3} P(\mathbf{r})exp(i2\pi\mathbf{q}_k \cdot \mathbf{r})d\mathbf{r} \tag{2}$$

2.2   Spherical Ridgelets

Spherical ridgelets are constructed by following the fundamental principles of wavelet theory [13,14]. Specially let $x \in \mathbb{R}_+$ and $\rho \in (0,1)$ be a positive scaling parameter. Further, let $\kappa(x) = exp\{-\rho x(x+1)\}$ be a Gaussian function, which we subject to a range of dyadic scaling which result in

$$\kappa(x) = \kappa(2^{-j}x) = exp\{-\rho \frac{x}{2^j}(\frac{x}{2^j}+1)\} \tag{3}$$

with $j \in \mathbb{N} := \{0,1,2,...\}$.

The semi-discrete frame $\mathbb{U}$ of spherical ridgelets can be defined as

$$\mathbb{U} := \{\psi_{j,v}|v \in \mathbb{S}^2, j = -1,0,1,2,...\} \tag{4}$$

where the spherical ridgelet functions $\psi_{j,v}$ at resolution $j \in \mathbb{N}$ and orientation $v \in \mathbb{S}^2$ is

$$\psi_{j,v} = \frac{1}{2\pi} \sum_{n=0}^{\infty} \frac{2n+1}{4\pi} \lambda_n(\kappa_{j+1}(n) - \kappa_j(n))P_n(\mathbf{u} \cdot \mathbf{v}), \forall \mathbf{u} \in \mathbb{S}^2 \tag{5}$$

where P_n denotes the Legendre polynomial of order n and $\kappa_{-1}(n)=0$, $\forall n$

$$\lambda_n = \begin{cases} 2\pi(-1)^{\frac{n}{2}} \cdot \frac{1 \cdot 3 \cdots (n-1)}{2 \cdot 4 \cdots n} & \text{if } n \text{ is even} \\ 0 & \text{if } n \text{ is odd} \end{cases} \tag{6}$$

when the $n = 0$, $\lambda_n = 2\pi$.

3   Proposed Model

3.1   3D Non-local Similarity Regularization

To improve the spatial resolution of the diffusion MR imaging, we adopt a 3D NLMs filter in [4,15] to capture the nonlocal similarity in each diffusion MRI. Different from the method in [4], We capture the 3D nonlocal similarity of the normalized diffusion MRI which directly determine the diffusion of water rather than the diffusion MRI. Based upon the philosophy of the NLMs, each target voxel $S(\mathbf{q}_k; \mathbf{r}_i)$ in the reconstructed high spatial resolution diffusion MRI of the kth direction can be represented as the weighted average of the voxels within its similarity neighborhoods, i.e.,

$$\hat{S}^*(\mathbf{q}_k; \mathbf{r}_i) = \sum_{j \in V_i} w_{ij}^k S^*(\mathbf{q}_k; \mathbf{r}_j) \tag{7}$$

where $\hat{S}^*(\mathbf{q}_k; \mathbf{r}_i)$ is the current estimation of $S^*(\mathbf{q}_k; \mathbf{r}_i)$, w_{ij}^k is the NLMs weights. For the kth 3D diffusion MRI, we could rewrite the Eq. (7) in a brief

$$\hat{S}_i^* = \sum_{j \in V_i} w_{ij} S_j^* \tag{8}$$

w_{ij} is defined as

$$w_{ij} = \frac{1}{Z_i} exp\{-\frac{\|N_{3D}(S_i^*) - N_{3D}(S_j^*)\|_2^2}{h^2}\} \tag{9}$$

where the constant Z_i ensures the sum of the weights is equal to 1. The $N_{3D}(S_i^*)$ and $N_{3D}(S_j^*)$ represents the 3D image patches around S_i^* and S_j^*, in practical we use $3 \times 3 \times 3$ voxels 3D windows. The similarity between patches is estimated within a restricted nonlocal volume V_i. With the nonlocal similarity in diffusion MRI, we require the estimation error if the weighted average and the upsampled image X as small as possible. Thus for each 3D diffusion MRI, the corresponding regularization term can be written as:

$$E_{nlms}(S^*) = \sum_{i \in \Omega} \| S_i^* - W_i S^* \|_2^2 \tag{10}$$

where Ω is the image grid of S^*, W_i is a row vector formed by the NLMs weights, which is defined as

$$W_i(j) = \begin{cases} w_{ij}, & j \in V_j \\ 0, & \text{otherwise} \end{cases} \tag{11}$$

We further rewrite (10) into the following concise form:

$$E_{nlms}(S^*) = \| (I - W)S^* \|_2^2 \tag{12}$$

where I is an identity matrix and W is the NLMs similar weight matrix defined by W_i in (11).

3.2 Sparse Representation Regularization

For the fixed $\mathbf{r}_0$, in q-space the $S^*(\mathbf{q}; \mathbf{r}_0)$ is the normalized diffusion signal at a b-shell along the direction $\mathbf{q} \in \mathbb{S}^2$. In practical settings, the $\mathbf{q}$ are discretized and restricted to a discrete set of orientations $\{\mathbf{q}_k\}_{k=1}^K$ which prescribes the acquisition of diffusion data in the form of K diffusion-encoded images $\{S_k^*\}_{k=1}^K$, which each $S_k^* : \mathbb{R}^3 \to \mathbb{R}^+$ corresponding to a given $\mathbf{q}_k$. In this case, for a fixed $\mathbf{r}_0$, the vector $[S_1^*(\mathbf{r}_0), S_2^*(\mathbf{r}_0), ..., S_K^*(\mathbf{r}_0)]^T \in \mathbb{R}^K$ represents a discretization of $S^*(\mathbf{q}|\mathbf{r}_0)$. For this purpose, we let $s(\mathbf{r}_0) \in R^K$ denotes the vector of diffusion signal whose kth entry is equal to $S_k^*(\mathbf{r}_0)$ and let the values of ψ_m for $m = 1, ..., M$ at the K acquisition locations be stored in a $K \times M$ matrix A defined as

$$A = \begin{bmatrix} \psi_1(u_1) & \psi_2(u_1) & \cdots & \psi_M(u_1) \\ \psi_1(u_2) & \psi_2(u_2) & \cdots & \psi_M(u_2) \\ \vdots & \vdots & \cdots & \vdots \\ \psi_1(u_K) & \psi_2(u_K) & \cdots & \psi_M(u_K) \end{bmatrix} \tag{13}$$

Each column of A is normalized through its $\mathbb{L}_2$-norm, to make all the spherical ridgelets have a unit norm. Thus the measurement s can be represented as

$$s(\mathbf{r}_0) = Ac(\mathbf{r}_0) + e(\mathbf{r}_0) \tag{14}$$

where $c(\mathbf{r}_0)$ denotes the vector of representation coefficients and $e(\mathbf{r}_0)$ denotes the measurement noise. Since our main intension is to recover the coefficients c using as few diffusion-encoding gradients as possible (implying $K \ll M$), there is an infinite number of solutions which would fit the constraint $\|A\{c\} - s\|_2 \ll \epsilon$. For each $\mathbf{r} \in \Omega_d$, the vector of representation coefficients $c(\mathbf{r})$ is sparse, we may write a compressed sensing criterion for the estimation of $c(\mathbf{r})$ as follows

$$\min_{c(\mathbf{r})} \|c(\mathbf{r})\|_1 \tag{15}$$

$$s.t. \|A\{c(\mathbf{r})\} - s(\mathbf{r})\|_2 \leq \epsilon. \tag{16}$$

independently at each $\mathbf{r} \in \Omega$. This setup has been successfully used in [14] to reconstruct the high angular resolution dMRI signals.

3.3 Our Proposed SSR-CS Approach

To gain the high spatial and angular resolution diffusion MRI, we should not only consider the similarity regularization of single 3D diffusion MRI but also the sparse representation regularization of the different direction 3D diffusion MRI. For reconstructing a collection of different directions image volumes $S = \{S_k^*\}_{k=1}^K$ with high spatial resolution, a unified SSR-CS approach is proposed. The super spatial and angular resolution problem can be deemed as

$$\hat{S} = \arg\min_{V>0,S} \|DHS - L\|_2^2 + \lambda_1 \sum_{i=1}^K \|(I - W)S\|_2^2 + \lambda_2 \|V\|_1 \tag{17}$$

$$s.t. \ S = AV$$

where L is a collection of low spatial resolution different directions images $L = \{L_k^*\}_{k=1}^K$; H and D stand for the blurring and down-sampling operations; A is the basis matrix introduced in compressed sensing section and each column vector of V is the representation coefficients at the corresponding voxel; the positive λ_1 and λ_2 determine the relative importance of data fitting terms versus the non-local similarity and sparse representation regularization terms. Note that it is not easy to directly solve the above problem because of the compound nature of the regularization it involves. we could rewrite the (18) into the following constrained optimization problem as

$$\hat{S} = \arg\min_{V>0,S} \|DHS - L\|_2^2 + \lambda_1 \sum_{i=1}^K \|(I - W)S\|_2^2 + \lambda_2\|V\|_1 + \lambda_3\|S - AV - q^t\|_2^2 \tag{18}$$

$$q^{t+1} = q^t + AV^{t+1} - r^{t+1} \tag{19}$$

The split Bregman approach [16] allows one to reduce (18) to a simpler form, the minimization can now be performed by sequentially minimizing with respect to S and V separately. The resulting iteration steps are

$$Step \ 1: S^{t+1} = \arg\min_S \|DHS - L\|_2^2 + \lambda_1\|S - \bar{S}\|_2^2 + \lambda_3\|S - AV^t - q^t\|_2^2 \tag{20}$$

$$(\bar{S}_i)^{t+1} = \sum_{j \in V_i} w(\bar{S}_i^{\,t}, \bar{S}_j^{\,t}) \bar{S}_j^{\,t} \tag{21}$$

$$Step\ 2:\ V^{t+1} = \arg\min_{V>0} \lambda_3 \|AV - (S^t - q^t)\|_2^2 + \lambda_2 \|V\|_1 \tag{22}$$

After we acquired the sparse coefficients, we can further compute the corresponding ODF image [13].

4 Experimental Results and Analysis

4.1 Construction of the Gold Standard

To validate the effectiveness of the proposed method, we conduct experiments on the simulated data sets proposed in [17]. In real clinical cases, diffusion MRI are often contaminated by rician noise. To validate the effectiveness of our model in high level noise condition and low level noise condition respectively, the simulated diffusion-encoded images were contaminated by two different levels of rician noise, giving rise to SNR of 40 db and 24 db. We use the following model in [14] to generate corresponding diffusion-encode images $\{S_k\}_{k=1}^K$ for a range of different values of K

$$S(\mathbf{q}; \mathbf{r}) = S(\mathbf{0}; \mathbf{r}) \sum_{i=1}^{M(\mathbf{r})} \alpha_i(\mathbf{r}) exp\{-b(\mathbf{q}^T D_i(\mathbf{r})\mathbf{q})\} \tag{23}$$

where $\alpha_i(\mathbf{r}) > 0$ are the positive weights obeying $\sum_{i=1}^{M(\mathbf{r})} \alpha_i(\mathbf{r}) = 1$, b is defined as a function of shape and amplitude of diffusion-encoding gradients, and $D_i(\mathbf{r})_{i=1}^{M(\mathbf{r})}$ are 3×3 diffusion tensors associated with $M(\mathbf{r})$ neural fiber tracts passing through the $\mathbf{r}$ coordinates.

The simulated set had a spatial dimension of $31{\times}31{\times}31$ voxels with 90 gradients directions in a quasi-uniform manner which is straightforward to adapt for sampling of the "northern" hemisphere. The set are consisted of some "fibres" crossing. $b = 2000\,\mathrm{s/mm^2}$ were used for data generation. The diffusion tensors $D_i(\mathbf{r})$ in (24) respectively were: $D_1 = diag([y, x, z]), D_2 = diag([x, z, y]), D_3 = diag([0, 0, 1]), D_4 = diag([1/\sqrt{3}, 1/\sqrt{3}, 1/\sqrt{3}])$. The orientations of diffusion flows (ODF) are shown in Fig. 1. The ODF are computed by the method in [18,19]. Note that the number of the diffusion components $M(\mathbf{r})$ varied between 1 and 3. One of the diffusion encoding images was shown in Fig. 2.

To again the low resolution diffusion image, we firstly blur and downsample the diffusion encoding image. A downsampling factor of 2 along each axis was used. Then we choose $K = 24$ of the original set of 90 diffusion gradients. Within the subset of the 24 diffusion gradients, their corresponding points in q-space were also in a quasi-uniform coverage of the northern hemisphere. Finally the chosen 24 simulated diffusion-encoded images were contaminated by two level of Rician noise, giving rise to SNR of 24 dB and 40 dB diffusion encoding LR images as shown in Figs. 3 and 4 to reconstruct the high spatial and angular resolution images.
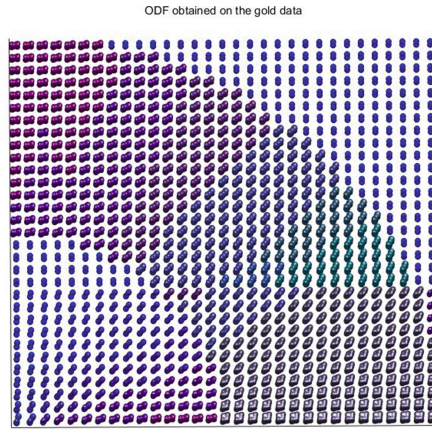
Fig. 1. The orientations of the original high angular diffusion flows
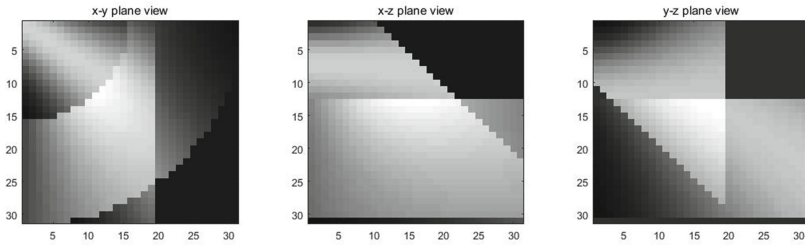
Fig. 2. Simulated 3D diffusion MRI and $\mathrm{SNR} = \infty\,\mathrm{dB}$
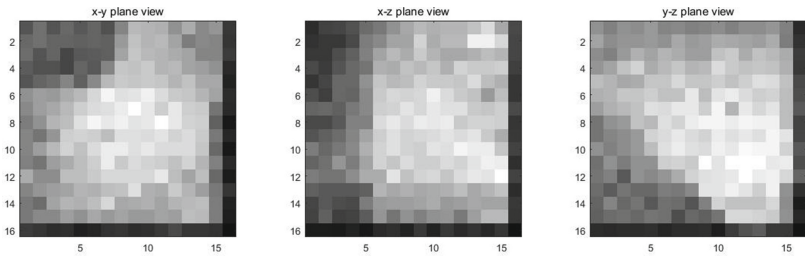
Fig. 3. Simulated downsampling 3D diffusion MRI and $\mathrm{SNR} = 24\,\mathrm{dB}$
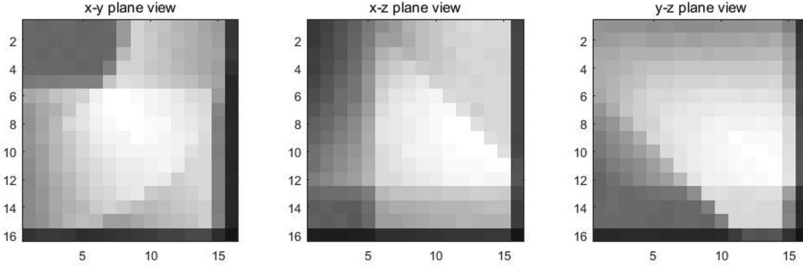
Fig. 4. Simulated downsampling 3D diffusion MRI and SNR = 40 dB

4.2   Experiment Results

To evaluate the quality of image reconstruction, we compare the proposed approach with cubic interpolation, B-spline interpolation. At the same time, the approach will also be compared to previously proposed patch-based superresolution methods (PBSR), the original PBSR method described in [15] used to reconstruct the normalized diffusion MRI instead of MRI was included in the comparison.

To evaluate the quality of reconstruction two different metrics were used, the usual Peak Signal-to-Noise Ratio (PSNR) and the percentage of generalized fractional anisotropy (GFA) were computed. The quality measures were estimated between the reconstructed HR images and the gold standard. The PSNR index was used to measure the spatial resolution quality and the GFA difference was used to measure the angular resolution quality. The experiment results were shown as follows.

Firstly we show the PSNR index in Tables 1 and 2 of our proposed method and the other methods compared when the LR data were in 24 dB and 40 dB. Then we should consider the angular index, i.e., GFA difference, see Tables 3 and 4.

From the results, we could see the proposed method has obvious advantage over the other methods when the LR data was in low SNR. When the LR data

Table 1. PSNR estimated between the gold standard and the reconstructed images from 24 dB data

	Cubic	Spline	PBSR	Proposed
PSNR (dB)	19.57	19.67	23.78	26.00

Table 2. PSNR estimated between the gold standard and the reconstructed images from 40 dB data

	Cubic	Spline	PBSR	Proposed
PSNR (dB)	19.79	20.00	31.79	31.92

Table 3. GFA difference estimated between the gold standard and the reconstructed images from 24 dB data

	PBSR	Proposed
GFA difference	2.46×10^{-2}	2.33×10^{-2}

Table 4. GFA difference estimated between the gold standard and the reconstructed images from 40 dB data

	PBSR	Proposed
GFA difference	3.21×10^{-2}	3.09×10^{-2}
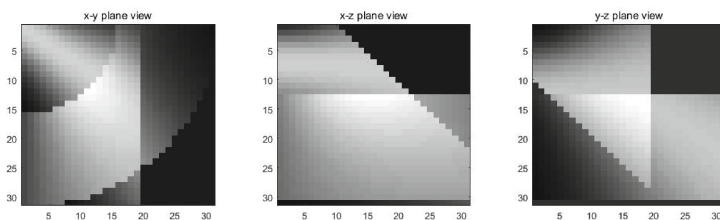
(a) Original high resolution 3D DWI
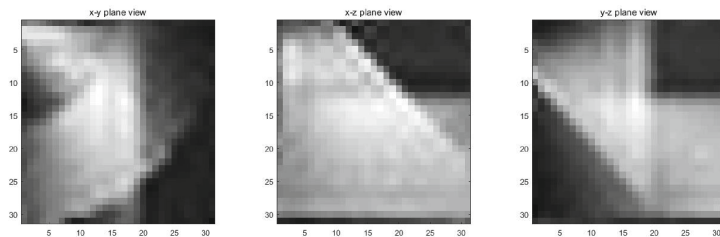
(b) PBSR reconstruction from 3D DWI 40db data
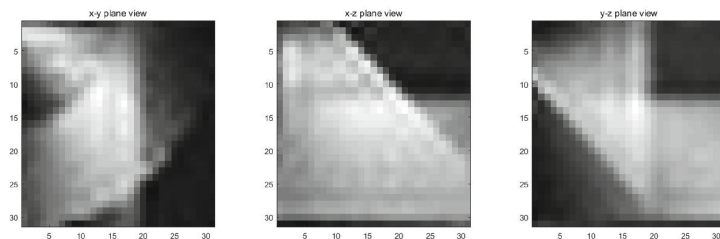
(c) Proposed method reconstruction from 3D DWI 40db data

Fig. 5. 3D DWI reconstruction using compared methods

was in high SNR, the proposed method is still best. Besides, the GFA difference index shows the proposed method is better than PBSR when the LR data was in 24 dB data and 40 dB data.
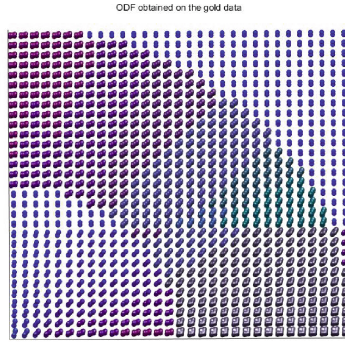
(a) The original ODF
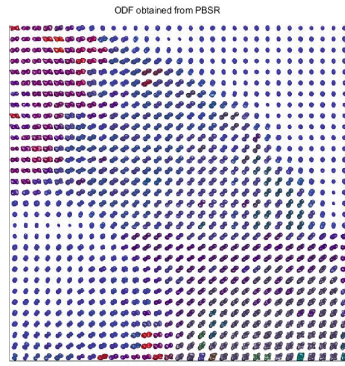
(b) The ODF of PBSR
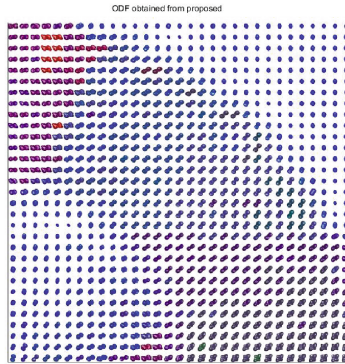
(c) The ODF of our method

Fig. 6. ODF using compared methods

The reconstructed 3D diffusion MRI from the 40 dB data using PBSR and our proposed method are shown in Fig. 5.

The reconstructed ODF from the 40 dB data using PBSR and our proposed method are shown in Fig. 6.

5   Conclusion

In this work, we investigated the possibility to increase diffusion MRI spatial resolution and angular resolution using a new method named SSR-CS. We combined the single image spatial superresolution and CS to propose a practical diffusion acquisition and reconstruction scheme that allows for obtaining HSAR diffusion MRI. The proposed technique is independent of scanner type and can be implemented on any clinically feasible scan time. We found that the proposed method could effectively reconstruct the high spatial and angular resolution diffusion MRI from the compared results.

We also note some limitations of the proposed method. When the LR diffusion MRI was in 40 dB, the proposed algorithm just improve 0.13 dB compared to the PBSR in PSNR. The advantage of the proposed method is not obvious. In the future we will focus on this aspect of the algorithm. At the same time, we should consider the speed of the algorithm because the clinical diffusion MRI were actually 4D data. The high dimension of the data will limit the speed of the super-resolution algorithm.

References

1. Stieltjes, B., Brunner, R.M., Fritzsche, K., Laun, F.: Diffusion Tensor Imaging. Springer, Heidelberg (2013)
2. Eriksson, S.H., Rugg-Gunn, F.J.: Diffusion tensor imaging in patients with epilepsy and malformations of cortical development. Brain **124**, 617–626 (2001)
3. Mori, S., van Zijl, P.: Fiber tracking: principles and strategies-a technical review. NMR Biomed. **15**, 468–480 (2002)
4. Coup, P., Manjn, J.V.: Collaborative patch-based super-resolution for diffusion-weighted images. NeuroImage **83**, 245–261 (2013)
5. Heidemann, R.M., Anwander, A.: k-space and q-space: combining ultra-high spatial and angular resolution in diffusion imaging using ZOOPPA at 7 T. NeuroImage **60**(2), 967–978 (2012)
6. Landman, B.A.: Resolution of crossing fibers with constrained compressed sensing using traditional diffusion tensor MRI. NeuroImage **59**(3), 2175–2186 (2012)
7. Scherrer, B., Gholipour, A., Warfield, S.K.: Super-resolution reconstruction to increase the spatial resolution of diffusion weighted images from orthogonal anisotropic acquisitions. Med. Image Anal. **16**, 1465–1476 (2012)
8. Poot, D.H.J., Jeurissen, B.: Super-resolution for multislice diffusion tensor imaging. Magn. Reson. Med. **69**, 103–113 (2013)
9. Van Steenkiste, G., Jeurissen, B.: Super-resolution reconstruction of diffusion parameters from diffusion-weighted images with different slice orientations. Magn. Reson. Med. **75**, 181–195 (2015)

10. Ning, L., Setsompop, K., Michailovich, O.: A joint compressed-sensing and super-resolution approach for very high-resolution diffusion imaging. NeuroImage **125**, 386–400 (2016)
11. Stejskal, E., Tanner, J.: Spin diffusion measurements: spin echoes in the presence of a time-dependent field gradient. J. Chem. Phys. **42**, 288–292 (1965)
12. Jansons, K.M., Alexander, D.C.: Persistent angular structure: new insights from diffusion MRI data. Dummy version. In: Taylor, C., Noble, J.A. (eds.) IPMI 2003. LNCS, vol. 2732, pp. 672–683. Springer, Heidelberg (2003). doi:10.1007/978-3-540-45087-0_56
13. Michailovich, O., Rathi, Y.: On approximation of orientation distributions by means of spherical ridgelets. IEEE Trans. Image Process. **19**(2), 461–477 (2010)
14. Michailovich, O., Rathi, Y., Dolui, S.: Spatially regularized compressed sensing for high angular resolution diffusion imaging. IEEE Trans. Med. Imaging, **30**(5), 1100–1115 (2011)
15. Manjn, J.V., Coup, P.: Non-local MRI upsampling. Med. Image Anal. **14**(6), 784–792 (2010)
16. Yin, W., Osher, S., Goldfarb, D., Darbon, J.: Bregman iterative algorithms for l1-minimization with applications to compressed sensing. SIAM J. Imaging Sci. **1**, 143–168 (2008)
17. Barmpoutis, A., Jian, B., Vemuri, B.C.: Adaptive kernels for multi-fiber reconstruction. In: Prince, J.L., Pham, D.L., Myers, K.J. (eds.) IPMI 2009. LNCS, vol. 5636, pp. 338–349. Springer, Heidelberg (2009). doi:10.1007/978-3-642-02498-6_28
18. Barmpoutis, A., Hwang, M.S.: Regularized positive-definite fourth order tensor field estimation from DW-MRI. NeuroImage **45**, 153–162 (2009)
19. Barmpoutis, A., Vemuri, B.C.: A unified framework for estimating diffusion tensors of any order with symmetric positive-definite constraints. In: 2010 IEEE International Symposium on Biomedical Imaging: From Nano to Macro, pp. 1385–1388. IEEE (2010)